Critical properties of the Anderson localization transition and the high-dimensional limit

E. Tarquini,[1,2,3] G. Biroli,[2,4] and M. Tarzia[1]

[1]*LPTMC, CNRS-UMR 7600, Sorbonne Université, 4 place Jussieu, 75252 Paris cédex 05, France*

[2]*Institut de physique théorique, Université Paris Saclay, CEA, CNRS, F-91191 Gif-sur-Yvette, France*

[3]*Université Paris-Sud, 91405 Orsay, France*

[4]*Laboratoire de Physique Statistique, Ecole Normale Supérieure, PSL Research University, 24 rue Lhomond, 75005 Paris, France*

(Received 14 December 2016; revised manuscript received 20 February 2017; published 10 March 2017)

In this paper we present a thorough study of transport, spectral, and wave-function properties at the Anderson localization critical point in spatial dimensions $d = 3, 4, 5, 6$. Our aim is to analyze the dimensional dependence and to assess the role of the $d \to \infty$ limit provided by Bethe lattices and treelike structures. Our results strongly suggest that the upper critical dimension of Anderson localization is infinite. Furthermore, we find that $d_U = \infty$ is a much better starting point compared to $d_L = 2$ to describe even three-dimensional systems. We find that critical properties and finite-size scaling behavior approach by increasing d those found for Bethe lattices: the critical state becomes an insulator characterized by Poisson statistics and corrections to the thermodynamics limit become logarithmic in the number N of lattice sites. In the conclusion, we present physical consequences of our results, propose connections with the nonergodic delocalized phase suggested for the Anderson model on infinite-dimensional lattices, and discuss perspectives for future research studies.

DOI: 10.1103/PhysRevB.95.094204

I. INTRODUCTION

Anderson localization (AL) is one of the most fundamental quantum phenomena. A system of noninteracting disordered electrons can be driven (e.g., by increasing the disorder strength or the energy) through a transition between a metallic (delocalized) phase and insulating (localized) phase, where diffusive transport is completely suppressed due to quantum interference [1]. After more than half a century of research [2], the subject is still very much alive as proved by recent experimental observation of AL in $1d$ [3] and $3d$ [4] atomic gases and for classical sound elastic waves in $3d$ [5].

The properties of AL in low-dimensional systems are by now very well established and understood. As predicted by the scaling theory of localization [6], all states are localized in $1d$ [7] and $2d$ (for system with orthogonal symmetry) by an infinitesimal amount of disorder. In fact, $d_L = 2$ is the lower critical dimension of the problem, where the so-called "weak localization" takes place [8].

During the last 40 years, a field theoretical approach [9] based on the replicated nonlinear σ model (NLσM) has been developed, and a perturbative ϵ expansion in $d = 2 + \epsilon$ dimensions has been pushed up to five loops [10]. These advances culminated in a functional (perturbative) renormalization group analysis [11] of the NLσM, which allowed computing the multifractal spectra of wave-function amplitudes at the AL critical point in $d = 2 + \epsilon$.

Nonetheless, despite about 60 years of intense research, there is still (almost) no available analytical approach for AL away from the low-dimensional limit and much less is known in higher dimensions. The main reasons for that are as follows:

(1) The absence of a small parameter: The critical disorder is of the same order (or even larger) than the bandwidth already in three-dimensional systems.

(2) The fact that AL is not associated with a conventional spontaneous symmetry breaking. Indeed, the order parameter which naturally arises in the field theoretical description is a function: the probability distribution of the local density of states (DOS) which develops heavy tails in the insulating phase due to very large and rare resonances. The average DOS instead does not show any sign of discontinuity at the transition.

These unconventional properties represent a challenge for analytical approaches. As a consequence numerical methods are still at the core of the advances in this topic [12].

AL in three dimensions was analyzed by many authors using numerical techniques for increasing system size, with the use of various scaling analyses and of different observables related both to transport properties [13,14] and to the statistics of energy levels [15,16] and wave-function coefficients [17,18]. In Ref. [19] the phase diagram in the energy-disorder plane was also calculated. For the model described in the next section (spinless electron in a uniformly distributed disordered potential) and for $E = 0$ (middle of the band) a localization transition is found at a critical value of the disorder $W_c \simeq 16.5$, separating a metallic phase, where wave functions are extended over the whole volume, from an insulating phase, where wave functions are exponentially localized around some particular sites. The quantity $\overline{\Upsilon_2} = \overline{\sum_i |\langle n|i\rangle|^4}$ (where $\langle n|i\rangle$ denotes the value of the eigenfunction $|n\rangle$ on site i), called the inverse participation ratio (IPR)—averaged over the disorder and over all eigenstates around $E = 0$—is often used to distinguish between these two regimes as $\overline{\Upsilon_2} \sim C/L^d$ in the extended phase and stays of $O(1)$ in the localized phase. Diffusion is completely suppressed in the insulating regime and the conductivity σ vanishes in the thermodynamic limit, while it stays finite in the metallic phase. The localization length, measuring the spatial extent over which wave functions are localized, diverges at the transition coming from the insulating phase. At present, the most precise numerical estimate of the critical exponent ν describing this divergence in $3d$—for systems with orthogonal symmetry—is $\nu = 1.58 \pm 0.01$ [14,17].

AL had a very strong impact also on random matrix theory (RMT). As a matter of fact, in the delocalized phase the level statistics on the scale of the mean-level spacing is expected to be described by RMT and generally corresponds to the

Gaussian orthogonal ensemble (GOE), whereas instead in the localized phase it is determined by Poisson statistics because wave functions close in energy are exponentially localized on very distant sites and hence do not overlap; thus, contrary to the GOE case, there is no level repulsion and eigenenergies are distributed similarly to random points thrown on a line. These ideas have been confirmed by numerical simulations in $3d$ [16].

Right—and only—at the critical point, level statistics is neither GOE nor Poisson [15,20] (it is instead characterized by a universal distribution which depends on the dimensionality) and wave-function amplitudes show a multifractal spectrum [18]—the critical eigenstates being neither extended nor localized reveal large fluctuations of wave-function amplitudes at all length scales.

A few recent accurate results are also available in $4d$ and $5d$ [21], based on the study of transport properties only. However, there are very few results on level statistics above dimension three [22] and no exact results for transport properties for $d > 5$ [23]. As we will discuss in the following, the reason for that is that running times of numerical algorithms increase very rapidly with the size of the system [more precisely, as L^{3d} for exact diagonalization (ED) and as L^{3d-2} for transfer matrix (TM) techniques]. This sets a very severe limitation on the system sizes which can be simulated as dimensionality is increased.

For these reasons, some basic questions of AL remain unanswered or debated. For instance, the existence of an upper critical dimension d_U is still an issue. Although several observations seem to indicate that d_U might be infinite [22,24,25], different propositions corresponding to $d_U = 4$, 6, and 8 have been put forward [26,27].

Another important and highly debated aspect is the relation with the infinite-d limit, corresponding to AL on treelike structures [28] and to other random matrix models with long-range hopping [29]. On the one hand, these models allow for an exact solution, making it possible to establish the transition point and the corresponding critical behavior [29–31]. On the other hand, however, the properties of the delocalized phase are very unusual, since they are affected by dramatic—and somehow unexpected—finite-size effects (FSEs) even very far from the critical point, which produce a strong nonergodic behavior in a crossover region where the correlation volume is larger than the accessible system sizes [29,32–37]. This makes the finite-size analysis of numerical data highly nontrivial [35,37], and has been interpreted by some authors [32–34] in terms of the existence of a new intermediate delocalized but nonergodic phase—which might be characterized by nonuniversal level statistics, anomalous scaling exponents of the IPR, and multifractality [38]—in a broad interval of disorder strength between the metallic (fully ergodic) phase and the insulating one.

This possibility is clearly very intriguing (although it appears to be in conflict with the analytical predictions of the SUSY formalism [31]), especially due to its relationship with many-body localization (MBL) [39], a fascinating new kind of phase transition between a low-temperature nonergodic phase—a purely quantum glass—and a high-temperature ergodic phase. Theoretical work strongly suggests that this phenomenon takes place for several disordered isolated interacting quantum systems, in particular disordered electrons [39] (it was also independently investigated in [40] to explain the quantum ergodicity transition of complex molecules). MBL can be pictorially interpreted as localization in the Fock space of Slater determinants, which play the role of lattice sites in a disordered (single-particle) Anderson tight-binding model. A paradigmatic representation of this transition [39–43] is indeed AL on a very high dimensional lattice, which for spinless electrons consist of an N-dimensional hypercube of 2^N sites.

All the open questions presented above motivated us to thoroughly analyze AL in high spatial dimensions. In the following we present a detailed study of the critical properties of AL in dimensions from 3 to 6 based on "exact" numerical methods (ED and TM techniques) and on an approximate strong-disorder renormalization group (SDRG) approach [44,45]. We focus on both the statistics of energy levels and wave-function coefficients and on transport properties. Our aim is to shed new light on the critical properties of AL and provide new insights to develop alternative analytical approaches to tackle this problem.

Our results support the idea that the upper critical dimension of AL is infinite. For instance, the critical exponent ν smoothly evolves from $\nu \to \infty$ in $d = 2$ to the value $\nu = 1/2$ in $d \to \infty$ predicted by the SUSY approach [46], showing no sign of saturation. Moreover, we find that the infinite-dimensional limit is a very good quantitative and qualitative starting point to describe AL even down to three dimensions. Expansions around the lower critical dimension, $d_L = 2$, instead give poorer results (even up to five loops). The higher the dimension the more AL is well described by a strong-disorder limit, as signaled by the fact that the critical values of all observables smoothly approach the ones of the localized phase as the dimensionality is increased—in $d \to \infty$ the critical states seem to correspond to an insulator, for which the statistics of energy levels is of Poisson type, and the multifractal spectrum of wave-function amplitudes takes its strongest possible form. Another strong indication of this fact is that the SDRG approach gives very accurate results in estimating the critical parameters in all dimensions $d \geqslant 3$.

We also show that FSEs become anomalously strong as d is increased. When d becomes large the scaling variable controlling finite-size scaling (FSS) is $|W - W_c|L^{1/\nu}$ and the leading corrections to FSS turn out to be proportional to L^y. Both ν and y depend weakly on the dimensions and tend to a constant when $d \to \infty$: $\nu \to 1/2$ and y stays roughly constant and close to -1. When reexpressed in terms of the system size $N = L^d$ these results suggest that corrections become logarithmic-like in N in the $d \to \infty$ limit. This behavior is drastically different from the one observed in conventional phase transitions, for which exists an upper critical dimension d_U such that for $d > d_U$ finite-size effects are governed by the scaling variable $|T - T_c|N^{1/\nu d_U}$ with corrections of the order of $N^{y'}$ (with some negative exponent y' independent of d).

The paper is organized as follows: In Sec. II we introduce the model and some basic definitions. In Sec. III we present our numerical results based on exact diagonalization and transfer matrix methods for dimensions from 3 to 6. In Sec. IV we discuss the SDRG approach, focusing especially on the properties of the flow close to criticality. In Sec. V

we give a brief summary of the results found and discuss their possible implications on the unusual properties of the delocalized phase observed in the Anderson model on treelike structures, which can be interpreted in terms of the extreme "quasilocalized" character of the AL critical point in $d \to \infty$, and of anomalously strong FSEs. Finally, in Sec. VI we present some concluding remarks and perspectives for future work.

II. THE MODEL

The model we focus on consists of noninteracting spinless electrons in a disordered potential:

$$\mathcal{H} = -t \sum_{\langle i,j \rangle} (c_i^\dagger c_j + c_j^\dagger c_i) - \sum_{i=1}^{N} \epsilon_i c_i^\dagger c_i, \tag{1}$$

where the second sum runs over all $N = L^d$ sites, and the first sum runs over all dL^d links of nearest-neighbor sites of the d-dimensional hypercubic lattice; $c_i^\dagger$, c_i are fermionic creation and annihilation operators, and t is the hopping kinetic energy scale, which we take equal to 1 throughout. The on-site energies ϵ_i are i.i.d. random variables uniformly distributed in the interval $[-W/2, W/2]$:

$$p(\epsilon) = \frac{1}{W}\,\theta\left(\frac{W}{2} - |\epsilon|\right), \tag{2}$$

W being the disorder strength. The model (1) has time reversal (and spin rotation) symmetry (also called *orthogonal* symmetry in the context of RMT). The common belief, supported by the scaling theory of localization [6], is that the transition is universal; i.e., it does not depend on microscopic details of the model such as the probability distribution of the on-site energies. However, it depends on the dimension and on the physical symmetry of $\mathcal{H}$.

In terms of RMT, the model (1) can be thought of as a sum of two matrices, $\mathcal{H} = \mathcal{C}^{(d)} + \mathcal{E}$ (i.e., a Schrödiger operator with random on-site potential): $\mathcal{C}^{(d)}$ is the (deterministic) connectivity matrix of the d-dimensional hypercube; $\mathcal{C}_{ij}^{(d)} = -t$ if sites i and j are connected and zero otherwise. $\mathcal{E}$ is a diagonal random matrix corresponding to the on-site energies, $\mathcal{E}_{ij} = \epsilon_i \delta_{ij}$.

In the following we will focus only on the middle of the spectrum, $E = 0$.

III. NUMERICAL RESULTS IN $d = 3, \ldots, 6$

In this section we present our numerical results in dimensions from 3 to 6 obtained from ED and a TM approach. We will focus first on transport properties and then on the statistics of energy gaps and wave-function amplitudes.

A. Transport properties

We consider a very long (length L_x) quasi-one-dimensional bar of cross section L^{d-1}, as sketched in Fig. 1. The system is open along the x direction, while periodic boundary conditions are enforced along the transverse directions. Such system, being quasi-1d, is always localized at any arbitrarily weak value of the disorder. The localization of electrons on this bar can be studied using the TM method. To this aim, we introduce

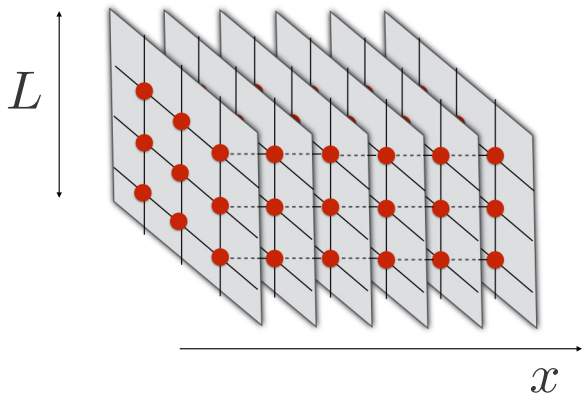

FIG. 1. Sketch of the quasi-one-dimensional bar along the x direction of cross section $L^{(d-1)}$.

the resolvent matrix, $\mathcal{G} = [z\mathcal{I} - \mathcal{H}]^{-1}$, where $z = E + i\eta$ with $\eta \to 0^+$ being the imaginary regulator, and express its matrix elements in terms of a Gaussian integral over a real auxiliary field:

$$\mathcal{G}_{lm} = -\frac{i}{Z} \int \prod_{i=1}^{N} d\phi_i\, \phi_l \phi_m\, e^{S[\phi_i]}, \tag{3}$$

where the action is given by

$$\begin{aligned} S[\phi_i] &= \frac{i}{2} \sum_{i,j=1}^{N} \phi_i (z\delta_{ij} - \mathcal{H}_{ij}) \phi_j \\ &= \frac{i}{2} \sum_i (E + i\eta + \epsilon_i)\phi_i^2 + i \sum_{\langle i,j \rangle} t_{ij} \phi_i \phi_j, \end{aligned} \tag{4}$$

and the "partition function" reads

$$Z = \int \prod_{i=1}^{N} d\phi_i\, e^{S[\phi_i]}. \tag{5}$$

We set $E = 0$ throughout, which corresponds to the band center. We set a finite positive value of η at $x = 0$ and $\eta = 0$ elsewhere inside the bar, at $x > 0$. This mimics putting the left boundary of the quasi-1d bar of Fig. 1 in contact with a thermal bath, and we study how dissipation propagates through the sample. The quasi-1d localization length, ξ_{1d}, can be easily measured from the exponential decay of the typical value of the imaginary part of the Green's function, $\exp[\overline{\ln \mathrm{Im}\mathcal{G}(x)}]$, as a function of x, averaged over all the sites of the xth layer and over several realizations of the disorder:

$$\overline{\ln \mathrm{Im}\mathcal{G}(x)} \simeq \text{const.} - \frac{x}{\xi_{1d}}. \tag{6}$$

Since Eq. (4) is a Gaussian action, in order to compute the left-hand side of Eq. (6) one can—at least formally—integrate over all the sites on a given layer x in Eq. (3), yielding an exact recursive relation expressing the Green's function on the subsequent layer, $x + 1$, in terms of the Green's function on the layer x in the absence of layer $x + 1$ (a kind of cavity equation for the whole layer):

$$[\mathcal{G}(x+1)]_{ij}^{-1} = \epsilon_{x,i}\delta_{ij} + t\mathcal{C}_{ij}^{(d-1)} - t^2 \mathcal{G}_{ij}(x), \tag{7}$$

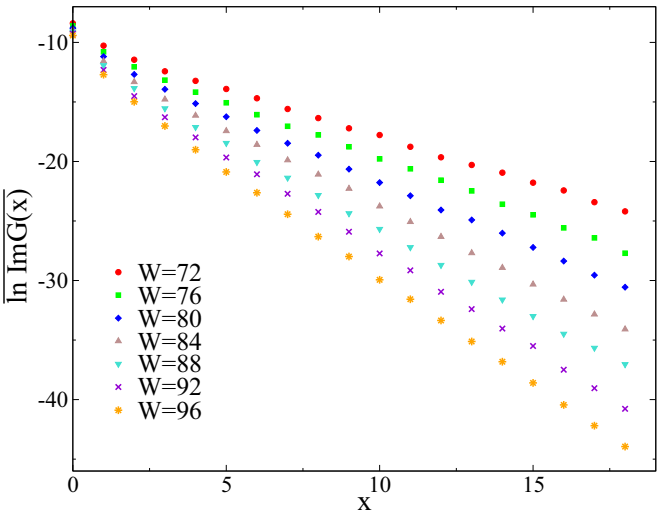

FIG. 2. $\overline{\ln \mathrm{Im}G(x)}$ as a function of x in 6 dimensions, for $L = 6$ and for several values of the disorder, showing that ξ_{1d} can be measured from Eq. (6) by linear fitting of the data at large enough x.

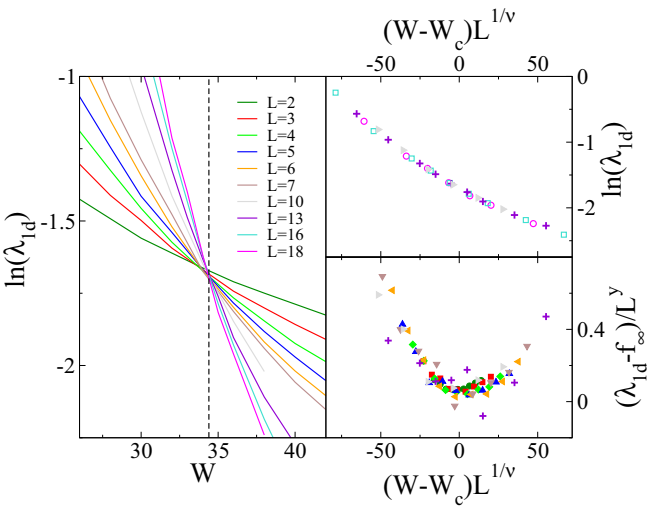

FIG. 3. Left panel: λ_{1d} as a function of the disorder W in $4d$ for several system sizes L from 2 to 18. The vertical dashed line spots the position of the critical point, $W_c \simeq 34.5$. Top-right panel: Finite-size scaling of the same data for L from 10 to 18, showing data collapse for $\nu \simeq 1.11$. Bottom-right panel: $\psi f_1 = (\lambda_{1d} - f_\infty)/L^y$ as a function of the scaling variable $(W - W_c)L^{1/\nu}$ for different sizes L from 2 to 7, showing data collapse for the same value as before of W_c and ν and for $y \simeq -1$.

where the index i runs over all the sites of layer x, $\epsilon_{x,i}$ is the random on-site energy on site i belonging to layer x, and $\mathcal{C}^{(d-1)}$ is the connectivity matrix of the transverse layers, i.e., the $(d-1)$-dimensional hypercube. This equation can be solved numerically by iteration, starting from the following initial condition at $x = 0$:

$$[\mathcal{G}(0)]_{ij}^{-1} = (\epsilon_{0,i} + i\eta)\delta_{ij} + t\mathcal{C}_{ij}^{(d-1)}. \tag{8}$$

In order to do this we need to invert the matrix $\mathcal{G}(x)$ layer by layer, which can be done by LU decomposition. Since the computer time required to perform this operation is proportional to the third power of the total number of sites of the matrix, $L^{3(d-1)}$, the running time of the TM algorithm scales as $L_x L^{3d-3} \sim L^{3d-2}$.

As an example, in Fig. 2 we plot $\overline{\ln \mathrm{Im}G(x)}$ as a function of x in 6 dimensions, for $L = 6$ and for several values of the disorder W, showing that ξ_{1d} can be measured using Eq. (6) by linear fitting of the data at large enough x. This is equivalent to the following definition of the quasi-$1d$ localization length via the transmission coefficient [13,47]:

$$\xi_{1d}^{-1} = -\lim_{L_x\to\infty} \frac{1}{2(L_x+1)} \ln \mathrm{Tr}|\langle 0|\mathcal{G}|L_x\rangle|^2,$$

where $\langle 0|\mathcal{G}|L_x\rangle$ denotes the L^{d-1}-dimensional matrix of the resolvent between the site states in the 0th and L_xth slice of the system (i.e., $\mathrm{Tr}|\langle 0|\mathcal{G}|L_x\rangle|^2$ is the probability for an electron to go from a site on the layer 0 to a site on the layer L_x). One can then work out the asymptotic behavior of ξ_{1d}: In the localized regime one expects that for L large enough ξ_{1d} saturates to the actual value of the localization length ξ of the d-dimensional system. Conversely, in the extended regime the wave traveling along the bar is evenly spread over the whole bar. The effective disorder seen by the wave in each layer is thus a statistical average over the disorder in the layer. One can show that the results of perturbation theory for $1d$ are also valid here, with the modified disorder $\tilde{W}^2 = W^2/L^{d-1}$ [47]. As a result, one expects that in the metallic phase ξ_{1d} grows as L^{d-1}, i.e., the number of (open) channels in the transverse direction. (Note that in this case the correlation length ξ is related to the resistivity of the d-dimensional system via $\sigma \propto 1/\xi^{d-2}$ [47].)

Hence, the good scaling variable is the dimensionless quasi-$1d$ localization length, defined as $\lambda_{1d} = \xi_{1d}/L$. This quantity is the inverse of the smallest positive Lyapunov exponent γ, and behaves as

$$\lambda_{1d} \simeq \begin{cases} (L/\xi)^{d-2} \propto \sigma L^{d-2} & \text{for } W < W_c, \\ \lambda_c & \text{for } W = W_c, \\ \xi/L & \text{for } W > W_c. \end{cases}$$

The left panels of Figs. 3, 4, and 5 show the behavior of (the logarithm of) the dimensionless quasi-$1d$ localization length λ_{1d} as a function of W for several system sizes in dimensions 4, 5, and 6, respectively. As expected, for small (resp. large) values of the disorder λ_{1d} grows (resp. decreases) as L is increased; for large enough sizes, the curves corresponding to different L cross at the critical point. However, the figures show the presence of systematic FSEs due to practical limitations on the system sizes: In $4d$ the crossing point shifts towards higher values of W by about 2.5% as L is increased from 2 to 18, while in $5d$ it moves towards lower values of the disorder (again by about 2.5%) when L goes from 2 to 9. FSEs become very strong in $6d$, where the crossing point shifts systematically to lower values of W by about 10% when L varies from 2 to 6. This gives a first qualitative indication of the fact that, differently from conventional phase transitions, FSEs for AL get stronger as the dimensionality is increased.

Such finite-size corrections must thus be taken into account in order to get accurate estimations of the critical values of the disorder strength and of the critical exponent. This can be done considering the presence of irrelevant scaling variables.

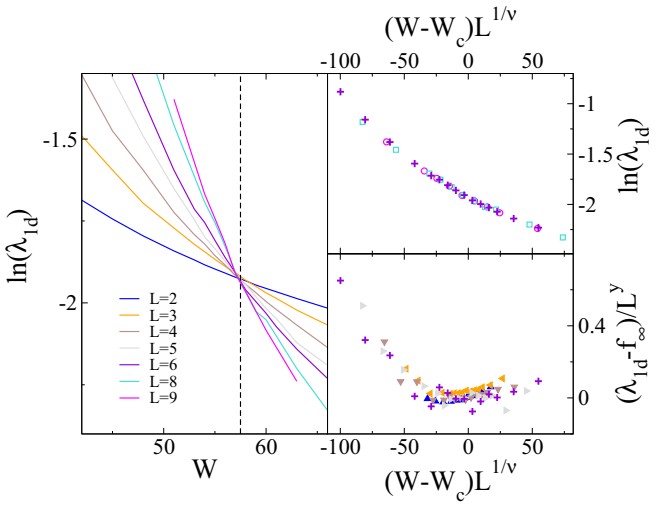

FIG. 4. Left panel: λ_{1d} as a function of the disorder W in $5d$ for several system sizes L from 2 to 9. The vertical dashed line spots the position of the critical point, $W_c \simeq 57.5$. Top-right panel: Finite-size scaling of the same data for L from 6 to 9, showing data collapse for $\nu \simeq 0.96$. Bottom-right panel: $\psi f_1 = (\lambda_{1d} - f_\infty)/L^y$ as a function of the scaling variable $(W - W_c)L^{1/\nu}$ for different sizes L from 2 to 6, showing data collapse for the same value as before of W_c and ν and for $y \simeq -1.2$.

More precisely, we follow [14,21] and suppose that the dependence of λ_{1d} on W and L can be described in terms of a scaling function:

$$\lambda_{1d}(W,L) = F(wL^{1/\nu}, \psi L^y), \tag{9}$$

where $w = (W - W_c)/W_c$ is the (dimensionless) distance from the critical point, ν is the critical exponent, ψ is the leading irrelevant scaling variable, and y is the smallest (in absolute value) irrelevant critical exponent (consistently, we should find $y < 0$ if ψ is irrelevant). For finite L there is no phase transition and F is a smooth function of its arguments. Hence, assuming that the irrelevant scaling variable is not dangerous (and for L large enough), one can expand Eq. (9) up to first order in ψL^y:

$$\lambda_{1d}(W,L) = f_\infty(wL^{1/\nu}) + \psi L^y f_1(wL^{1/\nu}). \tag{10}$$

In order to estimate W_c, ν, and y we then proceed in the following way:

(1) Since FSEs are negligible for L large enough, we suppose that one can obtain an approximate evaluation of the function $f_\infty(x)$ by performing a cubic fit of the numerical data for the largest available system sizes (in practice we use $L = 18$ and 16 in $d = 4$, $L = 9$ and 8 in $d = 5$, and $L = 6$ in $d = 6$). Note that the validity of this assumption must be verified *a posteriori*, since it depends on the value of the irrelevant exponent y, on $L_{\max}$, and on the form of the scaling function f_1.

(2) We plot the difference between the numerical data for $L < L_{\max}$ and the function f_∞ estimated in step (1), divided by L^y, as a function of the scaling variable $(W - W_c)L^{1/\nu}$. We determine the values of W_c, ν, and y that give the best data collapse of the curves corresponding to different values of L (see bottom-right panels of Figs. 3, 4, and 5), yielding an approximate estimation of (ψ times) the scaling function f_1 (which can also be approximated by a cubic fit).

(3) We plot λ_{1d} as a function of $(W - W_c)L^{1/\nu}$ for the largest sizes only, checking that our estimation of the critical parameters give a good data collapse (see top-right panels of Figs. 3, 4, and 5).

(4) Having estimated the scaling function ψf_1 and the critical parameters W_c, ν, and y in the previous steps, we can iteratively improve the estimation of f_∞ obtained in step (1) by performing a cubic fit of $\lambda_{1d}(W, L_{\max}) - \psi L_{\max}^y f_1(W, L_{\max})$, which takes into account finite-size corrections also for the largest system size in a self-consistent way. One can then repeat the whole process until it converges.

This analysis yields the following values for the critical parameters:

$d = 4$	$d = 5$	$d = 6$
$W_c = 34.5 \pm 0.2$	$W_c = 57.5 \pm 0.2$	$W_c = 83.5 \pm 0.4$
$\nu = 1.11 \pm 0.05$	$\nu = 0.96 \pm 0.06$	$\nu = 0.84 \pm 0.07$
$y = -1 \pm 0.1$	$y = -1.2 \pm 0.1$	$y = -1.4 \pm 0.2$

(11)

The results in $4d$ and $5d$ are in excellent agreement with the recent accurate estimations of [21], while our analysis provides the first direct calculation of the critical parameters for AL in six dimensions [48]. We also applied this method in $3d$ (not shown), yielding $W_c = 16.35 \pm 0.1$, $\nu = 1.57 \pm 0.02$, and $y = -1 \pm 0.1$, in excellent agreement with the results of Refs. [14,17]. Remarkably, the leading irrelevant exponent y seems to depend very weakly on the spatial dimension at least up to $6d$.

It is remarkable that finite-size corrections are governed by scaling variables [$(W - W_c)L^{1/\nu}$ and L^y] in which the *linear* size L enters raised to exponents (ν and y) that seem to have a finite limit when $d \to \infty$. This suggests a very different

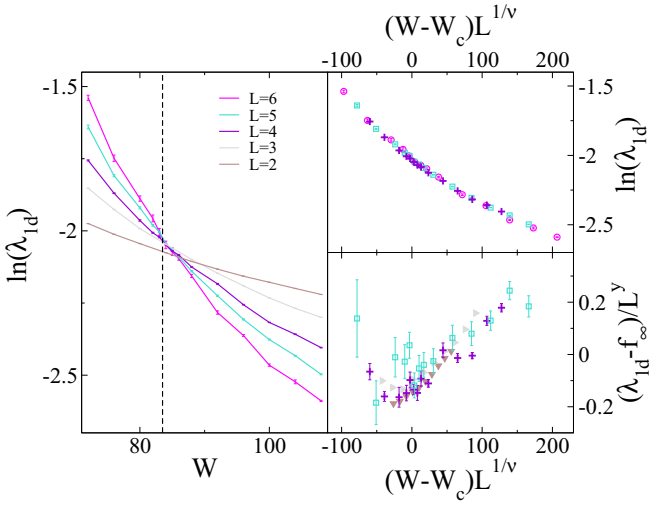

FIG. 5. Left panel: λ_{1d} as a function of the disorder W in $6d$ for several system sizes L from 2 to 6. The vertical dashed line spots the position of the critical point, $W_c \simeq 83.5$. Top-right panel: Finite-size scaling of the same data for L equal to 4, 5, and 6, showing data collapse for $\nu \simeq 0.84$. Bottom-right panel: $\psi f_1 = (\lambda_{1d} - f_\infty)/L^y$ as a function of the scaling variable $(W - W_c)L^{1/\nu}$ for different sizes L from 2 to 5, showing data collapse for the same value as before of W_c and ν and for $y \simeq -1.4$.

behavior from conventional phase transition where scaling variables instead are naturally expressed in terms of $N = L^d$. We will come back to this point in the conclusion.

B. Statistics of level spacings and of wave-function coefficients

In order to analyze the statistics of energy gaps and of wave-function amplitudes we have diagonalized the Hamiltonian (1) for dimensions from 3 to 6, for several system sizes L (with periodic boundary conditions), and for several values of the disorder strength W. For each L and W, we have averaged over several realizations of the on-site quenched disorder. Since we are interested in $E = 0$, we only focused on $1/16$ of the eigenstates centered around the middle of the band (we have checked that taking $1/32$ or $1/64$ of the states does not affect the results, but yields a poorer statistics). The computer time required for ED grows as the third power of the total number of sites of the matrix, L^{3d}. As a consequence, we can access slightly smaller system sizes with respect to the TM method. Still, one can simulate rather large values of L for low enough dimensions (e.g., $L_{\max} = 30$ for $d = 3$ and $L_{\max} = 13$ for $d = 4$), whereas one is instead limited to very small sizes as dimensionality is increased ($L_{\max} = 8$ for $d = 5$ and $L_{\max} = 5$ for $d = 6$). Note, however, that ED algorithms are faster if one only is interested in the eigenvalues and *not* in the eigenvectors. For this reason, in $d = 6$ we have been able to obtain some data for the statistics of energy gaps, for which the knowledge of the eigenfunctions is not necessary, also for $L_{\max} = 6$.

We have studied the statistics of level spacings of neighboring eigenvalues: $s_n = E_{n+1} - E_n \geqslant 0$, where E_n is the energy of the nth eigenstate in the sample. In the extended regime level crossings are forbidden. Hence the eigenvalues are strongly correlated and the level statistics is expected to be described by RMT (more precisely, several results support a general relationship between delocalization and the Wigner's surmise of the GOE). Conversely, in the localized phase wave functions close in energy are exponentially localized on very distant sites and do not overlap. Thus there is no level repulsion and eigenvalues should be distributed similarly to random points thrown on a line (Poisson statistics). In order to avoid difficulties related to the unfolding of the spectrum, we follow [49] and measure the ratio of adjacent gaps,

$$r_n = \frac{\min\{s_n, s_{n+1}\}}{\max\{s_n, s_{n+1}\}},$$

and obtain the probability distribution $\Pi(r)$, which displays a universal form depending on the level statistics [49]. In particular $\Pi(r)$ is expected to converge to its GOE and Poisson counterpart in the extended and localized regime [49,50], allowing us to discriminate between the two phases as $\bar{r}$ changes from $\bar{r}_{\rm GOE} \simeq 0.5307$ to $\bar{r}_P \simeq 0.3863$, respectively.

The GOE-Poisson transition can also be captured by correlations between nearby eigenstates such as the mutual overlap between two subsequent eigenvectors, defined as

$$q_n = \sum_{i=1}^{N} |\langle i|n\rangle||\langle i|n+1\rangle|.$$

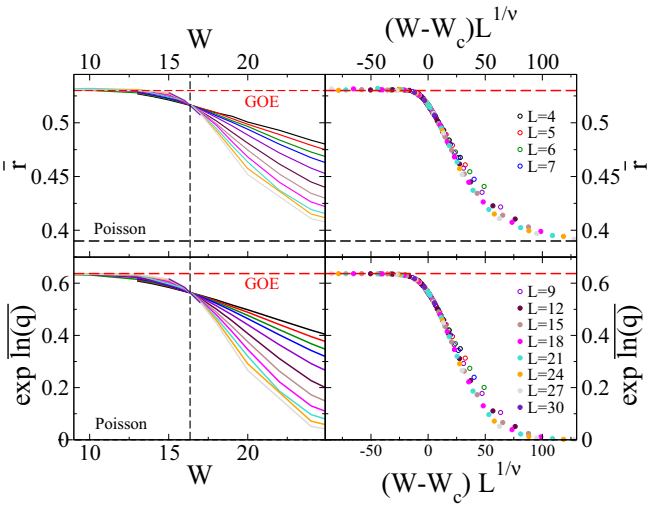

FIG. 6. $\bar{r}$ (top left) and $q^{\rm typ}$ (bottom left) as a function of the disorder W in $3d$ for several system sizes L from 4 to 30. The horizontal dashed lines correspond to the reference GOE and Poisson asymptotic values. The vertical dashed line spots the position of the AL transition, $W_c \simeq 16.35$. Finite-size scaling of the same data (top-right and bottom-right panels) showing data collapse obtained for $\nu \simeq 1.57$. Finite-size corrections to Eq. (12) are observed at small sizes (open symbols), and can be described by Eq. (10) with $y \simeq -1$.

In the GOE regime the wave-function amplitudes are i.i.d. Gaussian random variables of zero mean and variance $1/N$ [51]; hence $\overline{q}$ converges to $\overline{q}_{\rm GOE} = 2/\pi$. Conversely in the localized phase two successive eigenvector are generically peaked around very distant sites and do not overlap, and therefore $\overline{q}_P \to 0$ for $L \to \infty$. At first sight this quantity seems to be related to the statistics of wave-function coefficients rather than to energy gaps. Nonetheless, in all the random matrix models that have been considered in the literature up to now, one empirically finds that $\overline{q}$ is directly associated with the statistics of level spacings. The best example of that is provided by the generalization of the Rosenzweig-Porter random matrix model of [38], where there is a whole region of the parameter space where wave functions are delocalized but multifractal and strongly correlated, while the statistics of neighboring gaps is still described by the GOE ensemble. In this case one numerically finds that $\overline{q}$ converges to its GOE universal value $2/\pi$ irrespective of the fact that wave-function amplitudes are *not* i.i.d. Gaussian random variables of variance $1/N$.

In Figs. 6, 7, and 8 we show the behavior of the average value of the ratio of adjacent gaps, $\bar{r}$, and of the typical value of the mutual overlap between subsequent eigenvectors, $q^{\rm typ} = \exp[\overline{\ln q}]$, as a function of the disorder W, for several system sizes L, and for $d = 3$, 4, and 5 respectively. As expected, for small (resp. large) enough disorder we recover the universal values $\bar{r}_{\rm GOE} \simeq 0.5307$ and $q^{\rm typ}_{\rm GOE} = 2/\pi$ (resp. $\bar{r}_P \simeq 0.3863$ and $q^{\rm typ}_P \to 0$) corresponding to GOE (resp. Poisson) statistics. Data for different system sizes exhibit a crossing point around the critical points W_c, which coincide, within our numerical accuracy, with that obtained in the previous subsection from the analysis of the Lyapunov exponent, and are in good agreement with the ones reported in the literature [14,17,21]. One also finds that for large enough L the

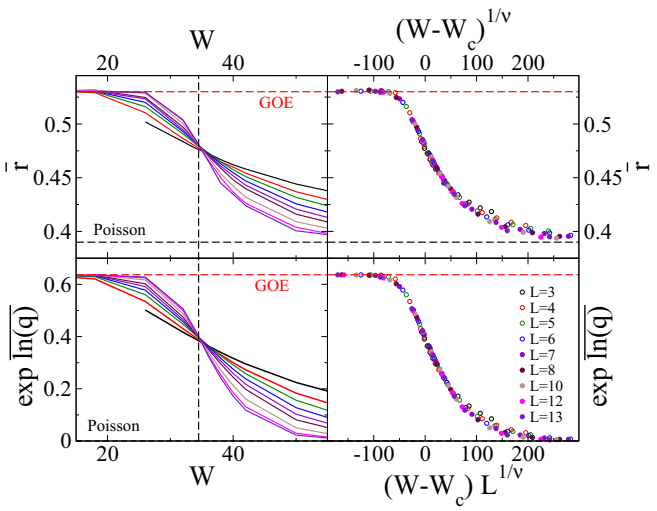

FIG. 7. $\bar{r}$ (top left) and $q^{\rm typ}$ (bottom left) as a function of the disorder W in $4d$ for several system sizes L from 3 to 13. The horizontal dashed lines correspond to the reference GOE and Poisson asymptotic values. The vertical dashed line spots the position of the AL transition, $W_c \simeq 34.5$. Finite-size scaling of the same data (top-right and bottom-right panels) showing data collapse obtained for $\nu \simeq 1.11$. Finite-size corrections to Eq. (12) are observed at small sizes (open symbols), and can be described by Eq. (10) with $y \simeq -1$.

whole probability distribution $\Pi(r)$ converges to its GOE and Poisson counterparts for $W < W_c$ and $W > W_c$, respectively. In the right panels of Figs. 6, 7, and 8, we show that for the largest accessible system sizes the dependence of $\bar{r}$ and $q^{\rm typ}$ on W and L can be described in terms of the scaling functions:

$$\bar{r}(W,L) = g_\infty(wL^{1/\nu}),$$
$$q^{\rm typ}(W,L) = h_\infty(wL^{1/\nu}), \tag{12}$$

with $w = (W - W_c)/W_c$. The values of ν are consistent, within our numerical incertitude, with the ones estimated using the TM method in the previous subsection, and are in perfect agreement with Refs. [14,17,21]. Deviations from Eq. (12) due to FSEs are clearly visible at small L, and can be described in terms of systematic corrections to the one-parameter scaling due to the presence of irrelevant scaling variables as explained above [see Eq. (10)]. The numerical values of the exponent y describing finite-size corrections to scaling for $\bar{r}$ and $q^{\rm typ}$ are compatible, within our numerical precision, with the ones reported in Eq. (11), confirming that the same sets of critical parameters describe the critical properties of level statistics and transport properties.

As already pointed out above, FSEs get stronger as dimensionality is increased. This effect is even more visible when level statistics is considered. In the left panel of Fig. 9 we show the behavior of $\bar{r}$ as a function of the disorder strength W, for L from 2 to 6 in six dimensions, showing dramatic FSEs: The crossing point shifts towards smaller values of W from about $W \sim 130$ to $W \sim 86$ as L is increased from 2 to 6, and it has not converged yet to W_c even for the largest available system size. Nevertheless, taking care carefully of finite-size corrections as explained in Sec. III A, one is able to show that the same set of critical parameters found from the analysis of the Lyapunov exponent ($W_c \simeq 83.5$, $\nu \simeq 0.84$, and $y \simeq -1.5$) yield a reasonably good finite-size scaling. This is

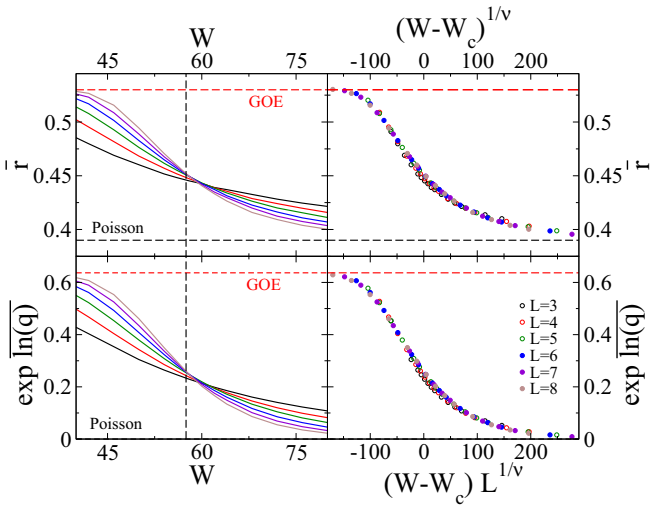

FIG. 8. $\bar{r}$ (top left) and $q^{\rm typ}$ (bottom left) as a function of the disorder W in $5d$ for several system sizes L from 3 to 8. The horizontal dashed lines correspond to the reference GOE and Poisson asymptotic values. The vertical dashed line spots the position of the AL transition, $W_c \simeq 57.5$. Finite-size scaling of the same data (top-right and bottom-right panels) showing data collapse obtained for $\nu \simeq 0.96$. Finite-size corrections to Eq. (12) are observed at small sizes (open symbols), and can be described by Eq. (10) with $y \simeq -1.2$.

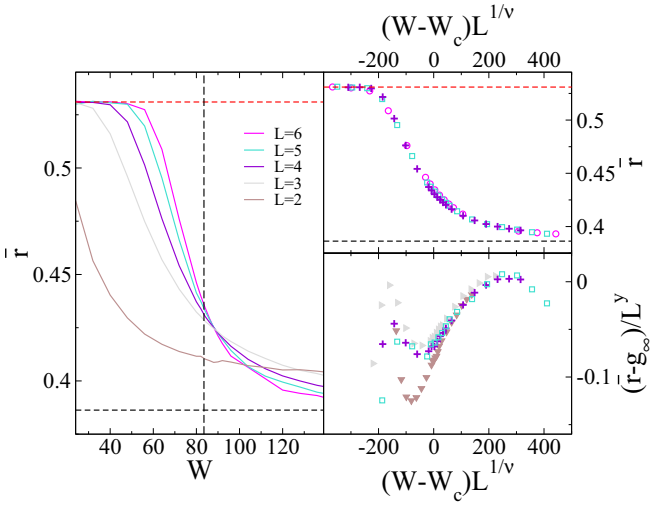

FIG. 9. Left panel: $\bar{r}$ as a function of the disorder W for several system sizes L from 2 to 6 in $6d$. The horizontal dashed lines correspond to the reference GOE and Poisson asymptotic values. The vertical dashed line spots the position of the AL transition, $W_c \simeq 83.5$. Top-right panel: Finite-size scaling of the same data for the largest system sizes only, $L = 4$, 5, and 6, showing data collapse for $\nu \simeq 0.84$. Bottom-right panel: $\psi g_1 = (\bar{r} - g_\infty)/L^y$ as a function of the scaling variable $(W - W_c)L^{1/\nu}$ for different sizes L from 2 to 5, showing a reasonably good data collapse for the same value as before of W_c and ν, and for $y \simeq -1.4$.

demonstrated by the top-right and bottom-right panels of Fig. 9, where the scaling functions g_∞ and (ψ times) g_1 are found from the data collapse of the numerical data in terms of the scaling variables $(W - W_c)L^{1/\nu}$. (We were not able to repeat the same analysis for $q^{\rm typ}$, since numerical data for the overlap between subsequent eigenvectors are available only up to $L = 5$.)

Analyzing fluctuations of eigenfunctions, we also focused on the (averaged) inverse participation ratio. The IPR of the eigenfunction $|n\rangle$ is defined as $\Upsilon_2^{(n)} = \sum_{i=1}^{L^d} |\langle i|n\rangle|^4$. In the full extended regime wave functions are uniformly spread over all the volume; thus $\langle i|n\rangle$ are random variables of order $1/\sqrt{L^d}$, due to normalization, and $\overline{\Upsilon_2}$ vanishes as C/L^d for $L \to \infty$—the prefactor C depends on the disorder strength W, approaching its GOE value equal to 3 deep in the metallic phase. Conversely in the localized phase wave functions are localized on $O(\xi^d)$ sites and $\overline{\Upsilon_2}$ approaches a constant value in the thermodynamic limit (in the infinite-disorder limit, $W \to \infty$, one has that $\overline{\Upsilon_2} \to 1$).

From the wave-function amplitudes obtained via ED, we have computed the typical value of the IPR, defined as $\Upsilon_2^{\rm typ} = \exp[\overline{\ln \Upsilon_2}]$, for several values of the disorder strength and of the system size L, and for dimensions from 3 to 5. The flowing fractal exponent β describing the scaling of $\Upsilon_2^{\rm typ}$ with L can then be approximately evaluated as

$$\beta(W,L) = -\frac{\ln \Upsilon_2^{\rm typ}(W,L) - \ln \Upsilon_2^{\rm typ}(W,L-1)}{d[\ln L - \ln(L-1)]}. \qquad (13)$$

In Fig. 10 we plot the numerical results for the exponent β as a function of W for several system sizes in four dimensions, showing a similar—although much less clean—behavior compared to the one found for the statistics of energy gaps: For $W < W_c$ one observes that β grows with L; its behavior is compatible with an approach towards 1 for L large enough, corresponding to full delocalized wave functions. Conversely, for $W > W_c$ the exponent β decreases as the system size is increased, and seems to approach 0 for large L, implying that $\Upsilon_2^{\rm typ} \to$ constant, as expected for localized eigenstates. For the largest available sizes, the curves corresponding to different values of L cross approximately around $W_c \simeq 34.5$. Although β is affected by much larger fluctuations and stronger FSEs compared to $\overline{r}$ and $q^{\rm typ}$, the same set of critical parameters found before ($W_c \simeq 34.5$, $\nu \simeq 1.11$, and $y \simeq -1$) yields a reasonably good data collapse of numerical data, as shown in the right panel of Fig. 10. Similar results are also found in dimensions 3 and 5 (not shown). This analysis cannot be performed in six dimensions, due to the fact that the IPR can be measured only up to $L_{\rm max} = 5$, which is not sufficiently large to take care in an accurate way of the strong FSEs.

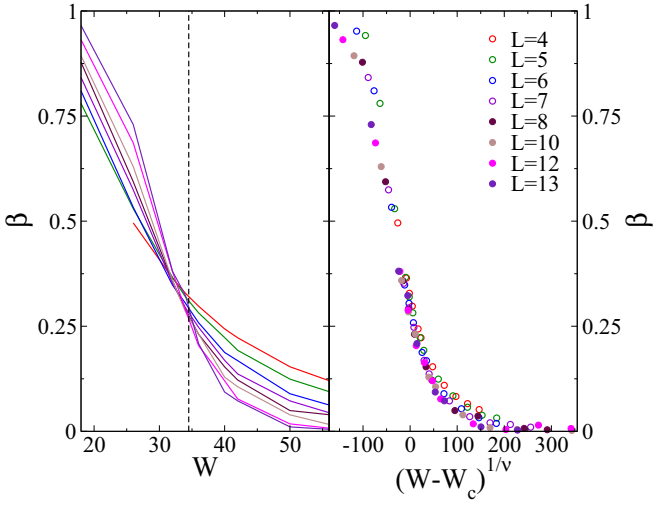

FIG. 10. Left panel: Flowing fractal exponent β describing the scaling of the typical value of the IPR with the system size for $d = 4$. The vertical dashed black line corresponds to the critical disorder $W_c \simeq 34.5$. Right panel: Finite-size scaling of the same data showing a reasonably good data collapse obtained for $\nu \simeq 1.11$. Strong finite-size corrections to the one-parameter scaling are observed at small sizes (open symbols), and can be described by Eq. (10) with $y \simeq -1$.

IV. STRONG-DISORDER RG

In this section we present our results based on the strong-disorder RG approach for AL recently introduced in [44,45]. The SDRG is an efficient real-space decimation procedure, consisting in integrating out iteratively the largest coupling constant in the Hamiltonian. The ideas behind this method reside in the seminal work of Ref. [52], and have been successfully applied to describe the critical and near-critical behavior of the random transverse-field Ising model and other random magnetic transitions [53], and have also been recently used in electronic systems [54].

In the case in which the strongest energy scale happens to be the on-site energy $|\epsilon_a|$ on site a, as sketched in the top panel of Fig. 11, one can perform the Gaussian integral over ϕ_a in Eq. (5), obtaining a RG transformation for the on-site energies on all the neighbors i of a and for the hopping amplitudes between all possible pairs of neighbors (ij) of a:

$$\epsilon_i \to \epsilon_i - \frac{t_{ai}^2}{\epsilon_a},$$

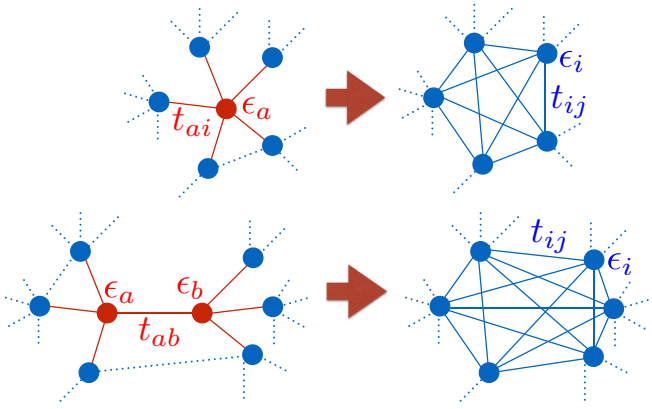

FIG. 11. Sketch of the SDRG decimation procedure for a site (top), and a bond (bottom) transformation. Dotted blue lines represent preexisting hopping amplitudes before decimation. Solid blue lines represent new or renormalized bonds. The on-site energies of all the neighbors of the decimated sites (blue circles) are renormalized as well.

$$t_{ij} \to t_{ij} - \frac{t_{ai}t_{aj}}{\epsilon_a}. \tag{14}$$

Similarly, if the strongest energy scale is the hopping amplitude $|t_{ab}|$ between sites a and b, as sketched in the bottom panel of Fig. 11, performing the Gaussian integrals over ϕ_a and ϕ_b in Eq. (5) yields the following RG transformation for the on-site energies on all the neighbors i of a and b and for the hopping amplitudes between all possible pairs of neighbors (ij) of a and/or b:

$$\begin{aligned}
\epsilon_i &\to \epsilon_i - \frac{\epsilon_a t_{bi}^2 - 2t_{ab}t_{ai}t_{bi} + \epsilon_b t_{ai}^2}{\epsilon_a\epsilon_b - t_{ab}^2}, \\
t_{ij} &\to t_{ij} - \frac{\epsilon_a t_{bi}t_{bj} - t_{ab}(t_{ai}t_{bj} + t_{aj}t_{bi}) + \epsilon_b t_{ai}t_{aj}}{\epsilon_a\epsilon_b - t_{ab}^2}.
\end{aligned} \tag{15}$$

Note that Eqs. (15) can be obtained using Eqs. (14) twice to eliminate first site a and then site b.

Equations (14) and (15) are in fact exact RG transformations, as it was first shown in [55]. However, the number of nonzero matrix elements grows very rapidly under RG due to the proliferation of new bonds (except, of course, in $1d$ [45]). This makes the numerical analysis unpractical. Several procedures have been proposed to solve this problem, which is also encountered in similar SDRG schemes for electronic systems [54] as well as for other disordered models such as the random transverse-field Ising model [53]. In this work we follow [44] and set a maximum coordination number $k_{\max}$ per site, throwing away most of the weak couplings. The rationale behind this procedure is that—at least in high enough dimension—the critical properties of AL are controlled by a strong-disorder limit, and the weak-coupling constants generated under RG are in fact "irrelevant".

In order to check whether or not this assumption is correct, it is important to analyze the accuracy of the results obtained using the SDRG and study their convergence with $k_{\max}$. We first focus on the average DOS, $\rho = -\mathrm{Tr}\,\mathrm{Im}\mathcal{G}/(\pi L^d)$.

We define the following quadratic form $\Gamma[\phi_i;\{\omega_i,\sigma_{ij},\kappa\}]$ of the auxiliary fields ϕ_i:

$$\Gamma[\phi_i;\{\omega_i,\sigma_{ij},\kappa\}] = \sum_i \omega_i\phi_i^2 + \sum_{i<j}\sigma_{ij}\phi_i\phi_j + i\kappa, \tag{16}$$

in terms of which the average DOS can be written as

$$\begin{aligned}
\rho = \frac{i}{\pi L^d Z}\,\mathrm{Im}\int\prod_{i=1}^{N} d\phi_i \\
\times\,\Gamma[\phi_i;\{\omega_i=1,\sigma_{ij}=0,\kappa=0\}]\,e^{S[\phi_i]},
\end{aligned} \tag{17}$$

where Z is defined in Eq. (5). When a site or a bond is integrated out under the RG transformations, some of the coefficients of Γ (i.e., those involving the neighboring sites of the decimated variables) must then be renormalized as well. Hence, although at the level of the initial conditions one has that $\omega_i = 1$ for all i, $\sigma_{ij} = 0$ for all (ij), and $\kappa = 0$ [see Eq. (17)], in order to compute the average DOS one needs to keep track of the flow of all the coefficients of Γ under RG. For example, when a given site, say site a, is decimated out, one has to renormalize the coefficients ω_i of all sites i neighbors of a, the coefficients σ_{ij} of all possible pairs of neighbors (ij) of a, as well as the value of the constant κ. This can be easily done by Gaussian integration:

$$\begin{aligned}
\omega_i &\to \omega_i + \frac{\omega_a t_{ai}^2}{\epsilon_a^2} - \frac{t_{ai}\sigma_{ai}}{\epsilon_a}, \\
\sigma_{ij} &\to \sigma_{ij} + \frac{2\omega_a t_{ai}t_{aj}}{\epsilon_a^2} - \frac{t_{ai}\sigma_{aj} + t_{aj}\sigma_{ai}}{\epsilon_a}, \\
\kappa &\to \kappa + \frac{\omega_a}{\epsilon_a}.
\end{aligned} \tag{18}$$

Similarly, when the hopping amplitude between sites a and b is eliminated, one can determine analogous RG relations for the coefficients of Eq. (16) using Eq. (18) twice, first on site a and then on site b. At the end of the RG, when all sites have been integrated out, ρ can be then obtained from Eq. (17) as (minus) the imaginary part of the final value of κ divided by πL^d.

We have computed the average DOS around the AL critical points for dimensions from 3 to 6 using this method for several values of $k_{\max}$, and compared its numerical value with the one obtained from ED, finding an excellent agreement even at small values of $k_{\max}$. In practice, already for $k_{\max} \gtrsim 60$ the average DOS obtained via the SDRG coincides within error bars and sample-by-sample with the one computed from ED for all the accessible system sizes and in all dimensions.

We turn now to transport properties. In particular, in the following we compare the results for the dimensionless quasi-$1d$ localization length computed from the TM approach as described in Sec. III A, with the ones obtained using the SDRG with different values of $k_{\max}$. More precisely, we consider the quasi-$1d$ bar of Fig. 1 and instead of solving Eq. (7) exactly via LU decomposition, we apply the SDRG to invert the matrix $[\mathcal{G}(x)]^{-1}$ in an approximate way, as explained in the following:

(1) We start from the layer at $x = 0$ which is in contact with an electron bath ($\eta > 0$) and integrate out progressively all the sites of the layer using Eqs. (14) and (15), eliminating iteratively the strongest energy scale, until no sites are left on the layer.

(2) In such a way, at the end of step (1) we end up with an approximate expression for the matrix element of the inverse cavity Green's function on the layer $x = 1$, $[\mathcal{G}(x=1)]^{-1}_{ij}$ (in the absence of the layer at $x = 2$). Then, knowing the left-hand side of Eq. (7), one can infer the matrix elements of the (cavity) Green's function on the layer $x = 0$, $\mathcal{G}_{ij}(x = 0)$, and compute the typical value of the imaginary part of its diagonal elements, $\overline{\ln \mathrm{Im}\mathcal{G}(x=0)}$.

(3) We then integrate out progressively all the sites of the layer $x = 1$ using Eqs. (14) and (15) to eliminate iteratively the strongest energy scale, yielding the matrix elements of the inverse cavity Green's function $[\mathcal{G}(x=2)]^{-1}_{ij}$ on the layer $x=2$ in the absence of the subsequent layer ($x = 3$), and use Eq. (7) "backwards" to infer $\mathcal{G}_{ij}(x = 1)$. We measure $\overline{\ln \mathrm{Im}\mathcal{G}(x=1)}$ and repeat the whole process until the layer $x = L_x$ is reached.

This procedure allows us to compute the dimensionless quasi-$1d$ localization length in a considerably faster way compared to exact LU decomposition. In Fig. 12 we plot the results for λ_{1d} at the AL critical point in dimension 6 ($W_c \simeq 83.5$) for different values of $k_{\max}$ and for $L = 3$ and 6, showing that for $k_{\max} \gtrsim 240$ the numerical values of λ_{1d} obtained via the SDRG approach converge, within

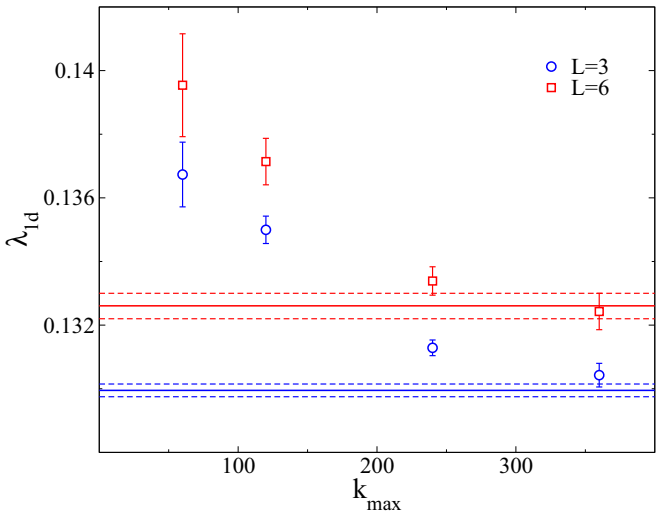

FIG. 12. Quasi-1d dimensionless localization length, λ_{1d}, obtained using the SDRG procedure for different values of $k_{\max}$, at the AL critical point, $W_c \simeq 83.5$, in 6 dimensions, and for $L = 3$ (blue circles) and $L = 6$ (red squares). The horizontal blue (resp. red) solid and dashed lines correspond to the average value of λ_{1d} and its fluctuations computed using the TM method for $L = 3$ (resp. $L = 6$), showing that for $k_{\max} \gtrsim 240$ the approximate SDRG results converge, within our numerical accuracy, to the exact values.

our numerical precision, with the ones obtained from exact techniques. Similar results are found in all dimensions down to $d = 3$ (not shown).

This analysis shows that the results obtained using the SDRG approach for both for the average DOS and the Lyapunov exponent converge already for reasonably small values of $k_{\max}$ to the exact ones in all spatial dimensions, at least close enough to the AL critical point [56]. Hence, the critical parameters found using the SDRG approach (for sufficiently large $k_{\max}$) coincide, within error bars, with the ones given in Eq. (11). Since the computer time required for an efficient algorithmic implementation of the SDRG procedure scales as $dL^d(\ln L)k_{\max}^2(\ln k_{\max})$, one can in principle apply this method to obtain very accurate results for much larger system sizes compared with the exact numerical techniques. The SDRG can then also be applied to study AL in dimensions larger than 6. This analysis goes beyond the scope of this work. Preliminary results in this direction have already been obtained in [44] up to $d = 10$.

In the last part of this section, we focus instead on the properties of the flow of the SDRG close to the AL critical point. More precisely, we study the evolution under RG of the probability distributions of the diagonal and off-diagonal matrix elements, $Q_\tau(\epsilon)$ and $R_\tau(t)$, respectively—the index τ corresponds to the RG "time". It is important to stress that these probability distributions do not contain *all* the relevant physical information on the system. For instance, they are insensitive to correlations between on-site energies and hopping amplitudes and/or spatial correlations between matrix elements which may be possibly generated during the flow. However, as we will discuss below, they can be still used to gather some useful qualitative insights on the critical properties of AL in high dimensions.

In the following, for simplicity, we will restrict ourselves to the case of real matrix elements (i.e., we set $\eta = 0$ on all the sites of the system). Similar results are obtained if one considers a finite (but small, e.g., $\eta \sim 10/L^d$) imaginary regulator and study, for instance, the flow of the probability distributions of the modulus of diagonal and off-diagonal matrix elements. At the AL critical point, the initial conditions for the probability distributions of on-site energies and hopping amplitudes are

$$Q_{\tau=0}(\epsilon) = \frac{1}{W_c}\,\theta\!\left(\frac{W_c}{2} - |\epsilon|\right),$$
$$R_{\tau=0}(t) = \frac{2d}{N-1}\,\delta(t-1) + \frac{N-1-2d}{N-1}\,\delta(t). \tag{19}$$

The critical disorder W_c is much larger than 1 already in three dimensions—and it grows very fast as d is increased (see Fig. 16). As a consequence, at the beginning of the RG, the strongest energy scales are provided by the sites with on-site energies close to the edges of the support of $Q_{\tau=0}(\epsilon)$. As these sites are integrated out, new hopping amplitudes are generated, and the two δ peaks of $R_{\tau=0}(t)$ acquire a finite support. Hence, as the RG time τ grows, $Q_\tau(\epsilon)$ shrinks and $R_\tau(t)$ broadens. When the support of the two distributions becomes approximately the same, we observe a stationary state [57].

The stationary distributions $Q_{\tau_\star}(\epsilon)$ and $R_{\tau_\star}(t)$ at the AL critical points are plotted in Fig. 13. Despite the fact that the initial conditions (19) change dramatically as d is increased,

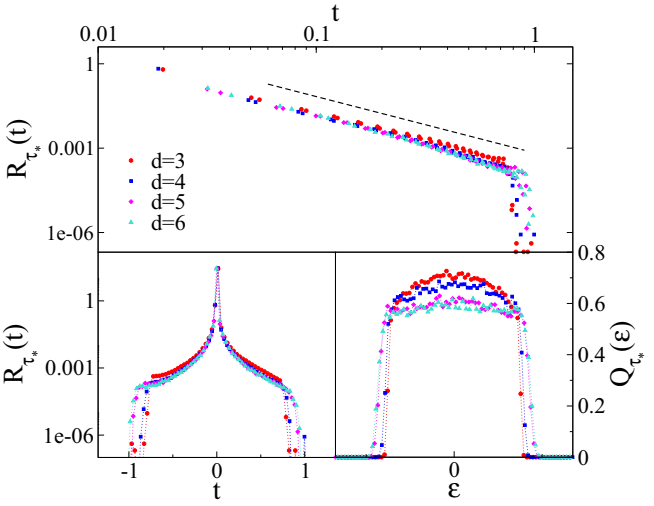

FIG. 13. Bottom-left and bottom-right panels: The stationary distributions $R_{\tau_\star}(t)$ and $Q_{\tau_\star}(\epsilon)$ at the AL critical points in dimensions from 3 to 6. The system size is $L = 33$ in $3d$, $L = 14$ in $4d$, $L = 8$ in $5d$, and $L = 6$ in $6d$, in such a way that the total number of sites is approximately the same, $N \sim 4 \times 10^4$, in all dimensions. The stationary state is reached for a RG time $\tau_\star$ such that the number of sites left in the system are approximately $1/8$ of the initial ones in $3d$, $1/16$ in $4d$, $1/26$ in $5d$, and $1/40$ in $6d$. The value of $k_{\max}$ is set to 360 in all dimensions. Top panel: The same data as in the bottom-left panel plotted in a log-log scale, showing the power law behavior of $R_{\tau_\star}(t) \sim t^{-\gamma}$ with $\gamma \simeq 2$ (black dashed line), for t smaller than a cutoff of $O(1)$.

we observe that $Q_{\tau_\star}(\epsilon)$ and $R_{\tau_\star}(t)$ are strikingly similar in all spatial dimensions from 3 to 6. This implies that the RG flow, and thus the critical properties of AL, are controlled by a fixed point which is very similar for all $d \geqslant 3$. As shown in the inset of Fig. 13, the tails of $R_\star(t)$ seem to be described by a power law, $R_{\tau_\star}(t) \sim t^{-\gamma}$, with an exponent $\gamma \simeq 2$ which is also roughly independent of d, and a cutoff for hopping amplitudes of $O(1)$, which seems to drift slowly to larger values of t as d is increased. Note however that for large d the initial conditions (19) get farther and farther from the stationary distributions. One needs then more and more RG steps to approach the stationary regime of the flow; i.e., $\tau_\star$ increases as d grows. For this reason, FSEs on $Q_{\tau_\star}(\epsilon)$ and $R_{\tau_\star}(t)$ also increase as d is increased since for $\tau = \tau_\star$ we are left with smaller systems and fewer matrix elements (see the caption of Fig. 13 for more details).

The power law tails of $R_{\tau_\star}(t)$ are reminiscent of a strong-disorder fixed point scenario [58], since they are related to the divergence of the variance of the distribution of the hopping amplitudes. However, the fact that the stationary distributions exhibit a cutoff on a scale of $O(1)$—which does not seem to be due to a FSE—implies that in fact all matrix elements stay of $O(1)$ and that the disorder does not grows under iterations of the RG transformations. Nonetheless, although at any finite d the fixed point is not of a "truly" infinite disorder type, the SDRG approach still provides an efficient and accurate approximation scheme. Furthermore, we find that the cutoff on the power law hopping distribution increases and possibly diverges in the large-d limit, suggesting that in this case one recovers a genuine infinite randomness fixed point scenario [58].

All in all, these observations provide a convincing indication of the fact that the properties of AL in high dimensions are governed by a "strong-disorder" fixed point, as already suggested in [35,44]. This idea is also supported by the results of the SUSY approach for the critical properties of AL on treelike structures and infinite-dimensional models [30,31], and will be discussed in more detail in the next section.

V. WEAK VERSUS STRONG COUPLING: ANALYSIS OF DIMENSIONAL DEPENDENCE

In this section we analyze the dimensional dependence at criticality of all observables discussed previously. As we shall show, approaching the lower critical dimension, $d_L = 2$, the critical point corresponds to weak disorder (or, equivalently, weak coupling in terms of the NLσM): when d approaches 2 the system at criticality is more and more metallic-like and described by the GOE universality class. On the contrary, when $d \to \infty$, the system at criticality is more and more insulating-like and described by the Poisson universality class. This section presents results supporting one of the main messages of this work, which is that the infinite-dimensional limit is a better starting point to describe systems in all dimensions down to $d = 3$.

1. Critical exponents and level statistics

We start by focusing on the critical exponent ν, whose behavior as a function of $1/d$ is plotted in Fig. 14. One clearly observes that ν continuously decreases from $\nu \to \infty$ in $d = 2$ to the value $\nu = 1/2$ in $d \to \infty$ predicted by the SUSY approach [46], showing no sign of saturation. This strongly indicates that the upper critical dimension of AL is infinite, as first suggested in [24] and more recently also in Refs. [22,25], in contrast, for instance, with the self-consistent theory of [27], which predicts $d_U = 4$ (turquoise dashed line). The perturbative analysis of the effective field theory based on the replicated NLσM has been carried to five-loop order in $\epsilon = d - 2$ [10], yielding

$$\nu = \frac{1}{\epsilon} - \frac{9}{4}\zeta(3)\epsilon^2 + \frac{27}{16}\zeta(4)\epsilon^3 + O(\epsilon^4). \qquad (20)$$

Such dimensional dependence of the critical exponent corresponds to the solid red line of Fig. 14, and yields a very poor agreement with the numerical results even in low dimensions. In fact, Eq. (20) violates the lower bound $\nu \geqslant 2/d$ based on the Harris criterion [59] (dashed-dotted magenta curve) already in $3d$. The straight dotted blue line in Fig. 14 is a linear fit corresponding to the first correction in $1/d$ from which we find

$$\frac{1}{\nu} \simeq 2 - \frac{4.75}{d}.$$

The quality of the fit shows that the first correction in $1/d$ performs much better than the expansion to the fifth order in $d - 2$ down to $d = 3$.

As mentioned above, these observations suggest that the critical properties of AL away from the lower critical

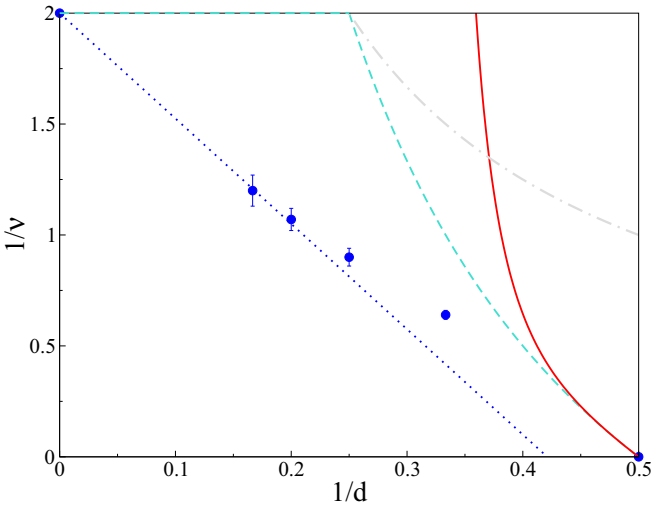

FIG. 14. Numerical values of the inverse of the critical exponent ν as a function of $1/d$ in dimensions from 3 to 6 (blue circles), showing a smooth behavior interpolating from $\nu \to \infty$ in $d = 2$ to $\nu = 1/2$ in $d \to \infty$ [46]. The turquoise dashed line shows the predictions of the self-consistent theory of [27], with $d_U = 4$. The dashed-dotted magenta line corresponds to the lower bound $\nu \geqslant 2/d$ provided by the Harris criterion [59]. The red solid line shows the dimensional dependence of ν obtained from a perturbative analysis of the NLσM to five-loop in $\epsilon = d - 2$ [10], Eq. (20). The straight dotted blue line is a linear fit corresponding to the first correction in $1/d$ from which we find $1/\nu \simeq 2 - 4.75/d$. The prediction of the semiclassical approach of Ref. [25], $\nu^{-1} = 2 - 4/d$, corresponds to the straight line interpolating from $\nu^{-1} = 2$ in $d \to \infty$ to $\nu^{-1} = 1$ in $d = 2$.

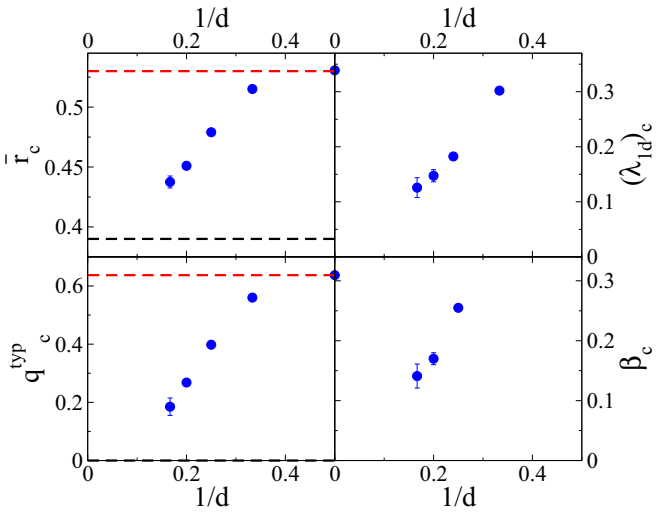

FIG. 15. Dimensional dependence of $\bar{r}_c$ (top-left panel), $q_c^{\rm typ}$ (bottom-left panel), $(\lambda_{1d})_c$ (top-right panel), and β_c at the AL critical point as a function of $1/d$. The dashed horizontal red (resp. black) lines correspond to the reference GOE (resp. Poisson values).

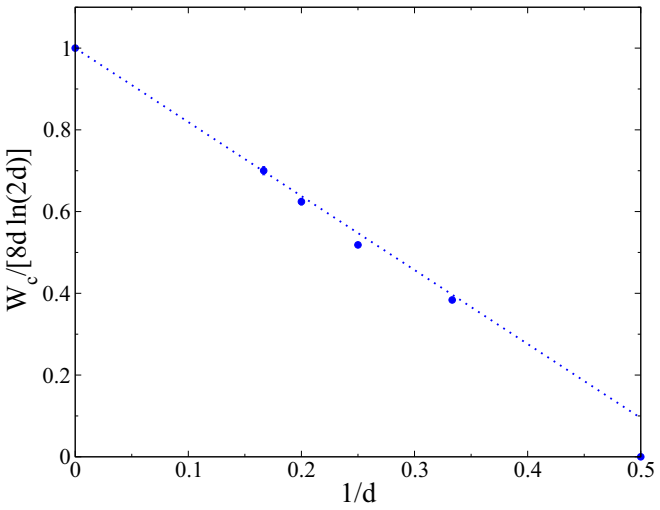

FIG. 16. Dimensional dependence of the critical value of the disorder strength, W_c, divided by $8d\ln(2d)$, which corresponds to the exact asymptotic behavior on treelike lattices in the large-connectivity limit [60]. The straight dotted blue line is a fit that takes into account corrections in $1/d$, from which we find $W_c/8d\ln(2d) \simeq 1 - 1.81/d$.

dimension might be governed by a strong-disorder regime, as suggested in [35,44]. This idea is fully confirmed by the analysis of the critical values and their dimensional dependence: In Fig. 15 we plot $\bar{r}_c$ (top-left panel), $q_c^{\rm typ}$ (bottom-left panel), $(\lambda_{1d})_c$ (top-right panel), and β_c (bottom-right panel) as a function of $1/d$. In $d = 2+\epsilon$ dimensions the critical point corresponds to weak disorder (or, equivalently, weak coupling in terms of the NLσM), which means that the critical level statistics is close to the GOE one. With increasing d the critical point moves continuously towards strong disorder (strong coupling), and $\bar{r}_c$ and $q_c^{\rm typ}$ approach the Poisson reference values, suggesting that the critical level statistics in the infinite-dimensional limit is of Poisson form, like in the localized phase. Similarly, β_c decreases as d is increased and seems to vanish in the $d \to \infty$ limit, implying that the IPR has a finite limit at the AL critical point in infinite dimensions, as predicted by the SUSY approach [31]. Finally, $(\lambda_{1d})_c$ is also a decreasing function of d, and smoothly approaches 0 for $d \to \infty$, confirming the idea that the AL critical point in infinite dimensions is strongly localized also as far as transport properties are concerned.

2. *Dimensional dependence of the critical disorder strength*

It is also interesting to study the dimensional dependence of the critical value of the disorder strength W_c. Figure 16 shows that W_c grows faster than d (which would be the natural scale set by the coordination number for conventional phase transitions) as the dimensionality is increased and seems to approach the curve $W_c/t \sim 4(2d-1)\ln(2d-1)$ for large d, which corresponds to the exact asymptotic behavior on treelike structures in the large-connectivity limit [28,60]. As for ν, we numerically evaluated corrections to the $d \to \infty$ result by a fit containing the first correction in $1/d$ (straight dotted blue line in Fig. 16). As before, the first correction performs impressively well down to $d = 3$. Recent predictions for the critical value of the disorder strength have been recently obtained in [23] up to $6d$, based on the forward scattering approximation [28], which provides an upper bound for W_c.

3. *Multifractality*

We finally turn to the analysis of the dimensional dependence of the critical multifractal spectra of wave-function amplitudes. Having in our disposition all the coefficients of the eigenvectors from ED, we can easily find the scaling behavior of all moments:

$$\Upsilon_q^{(n)} = \sum_{i=1}^{L^d} |\langle i|n\rangle|^{2q} \propto L^{-\tau(q)},$$

with the system size L. (Note that $\overline{\Upsilon_1} = 1$ due to the normalization condition, and $\overline{\Upsilon_2}$ is the IPR studied in Sec. III B.) In the metallic phase the wave-function amplitudes are of $O(1/L^d)$ and $\tau(q) = dq - 1$, whereas $\tau(q) = 0$ in the insulating regime. At criticality $\tau(q)$ is characterized by anomalous scaling exponents [61] which are the signatures of multifractal states. It is customary to introduce the singularity spectrum $f(\alpha)$, which denotes the fractal dimension of the set of points where the wave-function amplitude is $|\langle i|n\rangle|^2 \sim L^{-\alpha}$ [in our discrete system the number of such points $N(\alpha)$ scales as $L^{f(\alpha)}$]:

$$\Upsilon_q = \sum_{i=1}^{N} |\langle i|n\rangle|^{2q} \sim \int d\alpha \exp\{[f(\alpha) - q\alpha]\ln L\}.$$

Then, in the thermodynamic limit, the saddle point computation of Υ_q leads to the following Legendre transformation:

$$\alpha = \frac{d\tau(q)}{dq}, \qquad q = f'(\alpha), \qquad f(\alpha) = \alpha q - \tau(q). \quad (21)$$

$f(\alpha)$ is by definition a convex function of α. The value $q = 0$ is associated with the most probable value α_m of the

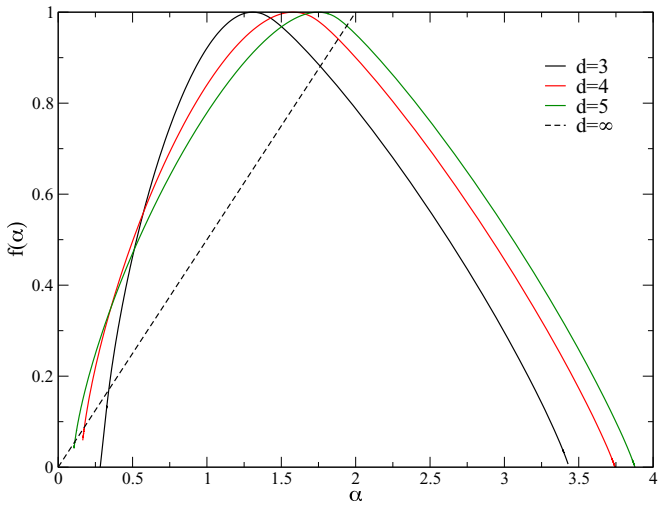

FIG. 17. Rescaled singularity spectrum $f(\alpha)/d$ as a function of α/d at the AL critical point in dimensions from 3 to 5. The dashed black straight line $f(\alpha) = \alpha/2$ for $\alpha \in [0,2]$ corresponds to the prediction of [61] in the $d \to \infty$ limit.

wave-function coefficients, where the singularity spectrum reaches its maximum, $f(\alpha_m) = d$. The value $q = 1$ is associated with the point α_1 such that $f(\alpha_1) = \alpha_1$, and $f'(\alpha_1) = 1$. A finite support $0 < \alpha_- < \alpha < \alpha_+$ where $f(\alpha) > 0$ in the $L \to \infty$ limit is a signature of multifractality, while for ergodic states, $f(\alpha) = -\infty$ unless for $\alpha = d$, where $f(d) = d$. From the ED data we have evaluated the typical value of the exponent $\tau(q)$ at the AL critical point as [18]

$$\tau_q^{\rm typ} = -\frac{d\,\overline{\ln \Upsilon_q}}{dL},$$

from which the spectrum of fractal dimensions $f(\alpha)$ can be determined applying the Legendre transformation, Eq. (21). Our numerical results in dimensions from 3 to 5 are plotted in Fig. 17, showing that the (rescaled) singularity spectrum of critical wave functions broadens as d is increased. In particular, the lower edge α_- of the support of $f(\alpha)$ seems to approach zero as d is increased and $f(\alpha)$ seems to approach (even though there is still a substantial difference) the infinite-dimensional prediction—observed on treelike lattices— which corresponds to the strongest possible form of multifractality and is represented by the straight line in Fig. 17 [61,62]. These observations support once again the extreme form of AL criticality in the $d \to \infty$ limit, where the critical states correspond to an insulator, are described by Poisson statistics, and their multifractal spectrum takes its strongest possible form.

4. The $d \to \infty$ limit and the Bethe lattice

We have shown above that the $d \to \infty$ limit is an extremely good starting point to analyze AL in finite dimensions. In the usual phase transitions the mean-field theory corresponding to the large-d limit is provided by the exact solution on completely connected models. In the case of AL instead completely connected lattices do not provide interesting results and the mean-field theory is instead believed to correspond to AL on Bethe lattices [28]. Our results confirm this expectation: the critical values of all observables tend for $d \to \infty$ to the ones of the localized phase, $\overline{r}_c = \overline{r}_P$, $q_c^{\rm typ} = 0$, $\beta_c = 0$, i.e., to the same critical behavior obtained for AL on Bethe lattices and treelike structures [30,31].

VI. CONCLUSION: PHYSICAL PICTURE AND PERSPECTIVES

In this last section, we discuss the implications of our results on the qualitative and quantitative understanding of AL on finite-dimensional lattices.

A. Anderson localization and rarefied conducting paths

The fact that the $d \to \infty$ limit provides a very good starting point to quantitatively describe AL suggests that the solution of AL on Bethe lattices is a good starting point to get a physical picture of AL on finite-dimensional lattices. Recently the delocalized phase of the Anderson model on treelike structures (and on related $d \to \infty$ random matrix models with long-range hopping [29]) has attracted a lot of attention [32–37]. Although it is still debated whether before the AL transition there is a nonergodic delocalized phase or a very strong crossover regime, it is clear that localization is related to the rarefaction of paths over which electrons can travel, as anticipated in [41,46]. Some authors advocate that this leads to a bona fide multifractal intermediate nonergodic but delocalized phase [33,34,41], others that this picture is valid below a certain scale that diverges (extremely fast) approaching the transition [35–37]. Although we do not see numerical evidence of an intermediate nonergodic delocalized phase for large d, the fact that in the scaling variables that govern finite-size scaling the linear size of the system, $L = N^{1/d}$, enters raised to powers that remain finite for $d \to \infty$ suggests that (1) quasi-one-dimensional paths are indeed the relevant geometrical objects for AL in high dimensions, and (2) scaling becomes logarithmic in N for $d \to \infty$ as found for treelike structures [29] and Bethe lattices [35,37]. In summary the idea of nonergodic transport along rarified paths is relevant even in finite dimensions even though possibly only on finite but very large length scales (on larger ones transport would be instead described by standard diffusion).

B. Expansion around the Bethe lattice

In the usual phase transitions two different expansions have been developed in order to describe the critical properties: one around the upper and another around the lower critical dimension. Our results clearly indicate that the former is a much better starting point for AL; see for example the comparison for the value of ν in Fig. 14. This is certainly a direction for future research and suggests that a $1/d$ expansion of the NLσM (in its replicated or SUSY formulation) could provide an excellent and controlled framework for AL. It would also be interesting to apply the SDRG to higher dimensions (preliminary results in this direction are already available [44] up to $d = 10$) as well as to implement alternative real-space RG schemes (such as the "resonance RG" method [63] and the Wegner flow equation approach [64]) introduced for the family of the power law random banded matrix ensembles, which have been shown

to be appropriate RG schemes in the strong-disorder limit. It seems that the only unique framework which would be capable of spanning the whole range from the infinitely weak disorder regime (in $d = 2 + \epsilon$) to the infinitely strong disorder limit (for $d \to \infty$) is a nonperturbative RG approach [65]. Developing such an RG method for AL is certainly worth future studies.

In summary, our work sheds new light on the critical properties of AL, and it characterizes the infinite-dimensional limit and stresses its relevance to describe AL even in three dimensions. Our results are also relevant for cases in which localization takes place on infinite-dimensional spaces, such as for many-body localized systems.

ACKNOWLEDGMENTS

We warmly thank V. Dobrosavljevic, Y. V. Fyodorov, V. Kravtsov, and G. Lemarié for useful inputs, remarks, and discussions. G.B. acknowledges support from the ERC grant NPRGGLASS and by a grant from the Simons Foundation (No. 454935, Giulio Biroli).

[1] P. W. Anderson, Phys. Rev. **109**, 1492 (1958).
[2] A. Lagendijk, B. V. Tiggelen, and D. S. Wiersma, Phys. Today **62**(8), 24 (2009).
[3] A. Aspect and M. Inguscio, Phys. Today **62**(8), 30 (2009); M. Greiner *et al.*, Nature (London) **415**, 39 (2002); **419**, 51 (2002).
[4] J. Chabé, G. Lemarié, B. Grémaud, D. Delande, P. Szriftgiser, and J. C. Garreau, Phys. Rev. Lett. **101**, 255702 (2008); F. Jendrzejewski, A. Bernard, K. Muller, P. Cheinet, V. Josse, M. Piraud, L. Pezze, L. Sanchez-Palencia, A. Aspect, and P. Bouyer, Nat. Phys. **8**, 398 (2012); B. Shapiro, J. Phys. A: Math. Gen. **45**, 143001 (2012).
[5] H. Hu, A. Strybulevych, J. H. Page, S. E. Skipetrov, and B. A. van Tiggelen, Nat. Phys. **4**, 945 (2008).
[6] E. Abrahams, P. W. Anderson, D. C. Licciardello, and T. V. Ramakrishnan, Phys. Rev. Lett. **42**, 673 (1979).
[7] N. F. Mott and W. D. Twose, Adv. Phys. **10**, 107 (1961).
[8] L. P. Gorkov, A. I. Larkin, and D. E. Khmelnitskii, JETP Lett. **30**, 228 (1979).
[9] F. J. Wegner, Z. Phys. B **35**, 207 (1979); L. Schaefer and F. J. Wegner, Z. Phys. B: Condens. Matter **38**, 113 (1980); K. B. Efetov, Adv. Phys. **32**, 53 (1983).
[10] S. Hikami, Prog. Theor. Phys. Suppl. **107**, 213 (1992).
[11] M. S. Foster, S. Ryu, and A. W. W. Ludwig, Phys. Rev. B **80**, 075101 (2009).
[12] For a review see B. Kramer and A. MacKinnon, Rep. Prog. Phys. **56**, 1469 (1993); See also P. Markoš, Acta Physica Slovaca **56**, 561 (2006).
[13] A. MacKinnon and B. Kramer, Phys. Rev. Lett. **47**, 1546 (1981); B. Kramer, M. Schreiber, and A. MacKinnon, Z. Phys. B **56**, 297 (1984); M. Schreiber, B. Kramer, and A. MacKinnon, J. Phys. C: Solid State Phys. **17**, 4111 (1984); B. Kramer, K. Broderix, A. MacKinnon, and M. Schreiber, Physica A **167**, 163 (1990); P. Cain, R. A. Römer, and M. Schreiber, Ann. Phys. (Leipzig) **8**, SI-33 (1999).
[14] K. M. Slevin and T. Ohtsuki, Phys. Rev. Lett. **82**, 382 (1999); New J. Phys. **16**, 015012 (2014).
[15] B. I. Shklovskii, B. Shapiro, B. R. Sears, P. Lambrianides, and H. B. Shore, Phys. Rev. B **47**, 11487 (1993).
[16] E. Hofstetter and M. Schreiber, Phys. Rev. B **48**, 16979 (1993); I. Kh. Zharekeshev and B. Kramer, *ibid.* **51**, 17239 (1995); Phys. Rev. Lett. **79**, 717 (1997); Ann. Phys. (Leipzig) **7**, 442 (1998); I. Varga, E. Hofstetter, M. Schreiber, and J. Pipek, Phys. Rev. B **52**, 7783 (1995).
[17] A. Rodriguez, L. J. Vasquez, K. Slevin, and R. A. Römer, Phys. Rev. Lett. **105**, 046403 (2010); Phys. Rev. B **84**, 134209 (2011).
[18] M. Schreiber and H. Grussbach, Phys. Rev. Lett. **67**, 607 (1991); M. Janssen, Int. J. Mod. Phys. B **08**, 943 (1994); H. Grussbach and M. Schreiber, Phys. Rev. B **51**, 663 (1995); L. J. Vasquez, A. Rodriguez, and R. A. Römer, *ibid.* **78**, 195106 (2008).
[19] B. Bulka, B. Kramer, and A. MacKinnon, Z. Phys. B: Condens. Matter **60**, 13 (1985).
[20] A. G. Aronov, V. E. Kravtsov, and I. V. Lerner, Phys. Rev. Lett. **74**, 1174 (1995).
[21] Y. Ueoka and K. Slevin, J. Phys. Soc. Jpn. **83**, 084711 (2014).
[22] A. M. García-García and E. Cuevas, Phys. Rev. B **75**, 174203 (2007).
[23] F. Pietracaprina, V. Ros, and Antonello Scardicchio, Phys. Rev. B **93**, 054201 (2016).
[24] A. D. Mirlin and Y. V. Fyodorov, Phys. Rev. Lett. **72**, 526 (1994); C. Castellani, C. D. Castro, and L. Peliti, J. Phys. A: Math. Gen. **19**, L1099 (1986).
[25] A. M. García-García, Phys. Rev. Lett. **100**, 076404 (2008).
[26] D. J. Thouless, J. Phys. C: Solid State Phys. **9**, L603 (1976); T. Lukes, *ibid.* **12**, L797 (1979); A. B. Harris and T. C. Lubensky, Phys. Rev. B **23**, 2640 (1981); J. P. Straley, *ibid.* **28**, 5393 (1983); I. Suslov, J. Exp. Theor. Phys. Lett. **63**, 895 (1996).
[27] D. Vollhardt and P. Wölfle, Phys. Rev. Lett. **48**, 699 (1982).
[28] R. Abou-Chacra, P. W. Anderson, and D. J. Thouless, J. Phys. C **6**, 1734 (1973).
[29] E. Tarquini, G. Biroli, and M. Tarzia, Phys. Rev. Lett. **116**, 010601 (2016).
[30] K. B. Efetov, Sov. Phys. JETP **61**, 606 (1985); M. R. Zirnbauer, Phys. Rev. B **34**, 6394 (1986); Nucl. Phys. B **265**, 375 (1986); K. B. Efetov, Sov. Phys. JETP **65**, 360 (1987); **66**, 634 (1987); J. J. M. Verbaarschot, Nucl. Phys. B **300**, 263 (1988); A. D. Mirlin and Y. V. Fyodorov, *ibid.* **366**, 507 (1991).
[31] Y. V. Fyodorov and A. D. Mirlin, J. Phys. A **24**, 2219 (1991); Phys. Rev. Lett. **67**, 2049 (1991); Y. V. Fyodorov, A. D. Mirlin, and H.-J. Sommers, J. Phys. I **2**, 1571 (1992).
[32] G. Biroli, A. C. Ribeiro-Teixeira, and M. Tarzia, arXiv:1211.7334.
[33] A. De Luca, B. L. Altshuler, V. E. Kravtsov, and A. Scardicchio, Phys. Rev. Lett. **113**, 046806 (2014); A. De Luca, A. Scardicchio, V. E. Kravtsov, and B. L. Altshuler, arXiv:1401.0019.
[34] B. L. Altshuler, E. Cuevas, L. B. Ioffe, and V. E. Kravtsov, Phys. Rev. Lett. **117**, 156601 (2016); B. L. Altshuler, L. B. Ioffe, and V. E. Kravtsov, arXiv:1610.00758.
[35] K. S. Tikhonov, A. D. Mirlin, and M. A. Skvortsov, Phys. Rev. B **94**, 220203(R) (2016).

[36] K. S. Tikhonov and A. D. Mirlin, Phys. Rev. B **94**, 184203 (2016).
[37] I. Garcia-Mata, O. Giraud, B. Georgeot, J. Martin, R. Dubertrand, and G. Lemarié, arXiv:1609.05857.
[38] V. E. Kravtsov, I. M. Khaymovich, E. Cuevas, and M. Amini, New J. Phys. **17**, 122002 (2015).
[39] D. M. Basko, I. L. Aleiner, and B. L. Altshuler, Ann. Phys. **321**, 1126 (2006).
[40] D. E. Logan and P. G. Wolynes, Phys. Rev. B **36**, 4135 (1987); J. Chem. Phys. **93**, 4994 (1990); R. Bigwood, M. Gruebele, D. M. Leitner, and P. G. Wolynes, Proc. Natl. Acad. Sci. USA **95**, 5960 (1998).
[41] B. L. Altshuler, Y. Gefen, A. Kamenev, and L. S. Levitov, Phys. Rev. Lett. **78**, 2803 (1997).
[42] Ph. Jacquod and D. L. Shepelyansky, Phys. Rev. Lett. **79**, 1837 (1997).
[43] A. De Luca and A. Scardicchio, Europhys. Lett. **101**, 37003 (2013).
[44] H. Javan Mard, J. A. Hoyos, E. Miranda, and V. Dobrosavljevic, arXiv:1412.3793.
[45] H. Javan Mard, J. A. Hoyos, E. Miranda, and V. Dobrosavljevic, Phys. Rev. B **90**, 125141 (2014).
[46] K. B. Efetov, Zh. Eksp. Teor. Fiz. **94**, 357 (1988); Physica A **167**, 119 (1990); *Supersymmetry in Disorder and Chaos* (Cambridge University Press, Cambridge, 1997).
[47] A. MacKinnon and B. Kramer, Z. Phys. B: Condens. Matter **53**, 1 (1983).
[48] Note, however, that in order for the assumption in (1) to be correct, one has to check self-consistently that $\psi L_{\max}^{y} f_1(0) \ll f_\infty(0)$. While this seems fully justified in $d = 4$ and $d = 5$, it might be slightly less well grounded in $d = 6$. Hence, the critical disorder W_c and the absolute value of the exponent y might be overestimated in six dimensions.
[49] V. Oganesyan and D. A. Huse, Phys. Rev. B **75**, 155111 (2007).
[50] Y. Y. Atas, E. Bogomolny, O. Giraud, and P. Vivo, J. Phys. A: Math. Gen. **46**, 355204 (2103).
[51] C. Porter and R. Thomas, Phys. Rev. **104**, 483 (1956).
[52] D. S. Fisher, Phys. Rev. Lett. **69**, 534 (1992).
[53] F. Iglói and C. Monthus, Phys. Rep. **412**, 277 (2005); O. Motrunich, S.-C. Mau, D. A. Huse, and D. S. Fisher, Phys. Rev. B **61**, 1160 (2000); I. A. Kovács and F. Iglói, *ibid.* **83**, 174207 (2011).
[54] C. Monthus and T. Garel, Phys. Rev. B **80**, 024203 (2009).
[55] H. Aoki, J. Phys. C **13**, 3369 (1980).
[56] It is natural to expect that the accuracy of the SDRG gets worse at small disorder strength, deep into the metallic phase.
[57] In practice, we observe that in all dimensions from 3 to 6 this happens when the support of the probability distributions of the diagonal and off-diagonal elements becomes of $O(1)$. As τ is further increased, the number of matrix elements left in the systems becomes very small and the stationary distribution is wiped out. However, this is a finite-size effect which could in principle be avoided taking larger and larger systems.
[58] D. S. Fisher, Phys. Rev. B **51**, 6411 (1995).
[59] J. T. Chayes, L. Chayes, D. S. Fisher, and T. Spencer, Phys. Rev. Lett. **57**, 2999 (1986); B. Kramer, Phys. Rev. B **47**, 9888 (1993).
[60] V. Bapst, J. Math. Phys. **55**, 092101 (2014).
[61] F. Evers and A. D. Mirlin, Rev. Mod. Phys. **80**, 1355 (2008); F. Evers, A. Mildenberg, and A. D. Mirlin, Phys. Status Solidi B **245**, 284 (2008).
[62] We were not able to compute the singularity spectrum in 6 dimensions due to practical limitations in the system sizes.
[63] A. D. Mirlin and F. Evers, Phys. Rev. B **62**, 7920 (2000); L. S. Levitov, Phys. Rev. Lett. **64**, 547 (1990).
[64] F. Wegner, Ann. Physik **506**, 77 (1994); S. D. Glazek and K. G. Wilson, Phys. Rev. D **48**, 5863 (1993); V. L. Quito, P. Titum, D. Pekker, and G. Refael, Phys. Rev. B **94**, 104202 (2016).
[65] J. Berges, N. Tetradis, and C. Wetterich, Phys. Rep. **363**, 223 (2002).